Transverse wobbling: A collective mode in odd-*A* triaxial nuclei

S. Frauendorf[1,*] and F. Dönau[2,†]

[1]*Department of Physics, University of Notre Dame, South Bend, Indiana 46556, USA*

[2]*Institut für Strahlenphysik, Helmholtz-Zentrum Dresden-Rossendorf, 01314 Dresden, Germany*

(Received 7 October 2013; revised manuscript received 17 November 2013; published 27 January 2014)

The wobbling motion of a triaxial rotor coupled to a high-j quasiparticle is treated semiclassically. Longitudinal and transverse coupling regimes can be distinguished depending on, respectively, whether the quasiparticle angular momentum is oriented parallel or perpendicular to the rotor axis with the largest moment of inertia. Simple analytical expressions for the wobbling frequency and the electromagnetic $E2$ and $M1$ transition probabilities are derived assuming rigid alignment of the quasiparticle with one of the rotor axes and harmonic oscillations (HFA). Transverse wobbling is characterized by a decrease of the wobbling frequency with increasing angular momentum. Two examples for transverse wobbling, ^{163}Lu and ^{135}Pr, are studied in the framework of the full triaxial particle-rotor model and the HFA. The signature of transverse wobbling, decreasing wobbling frequency, and enhanced $E2$ interband transitions, is found in agreement with experiment.

DOI: 10.1103/PhysRevC.89.014322 PACS number(s): 21.10.Re, 23.20.Lv, 27.70.+q

I. INTRODUCTION

Textbooks on classical mechanics (see, e.g., [1]) discuss the motion of a rigid rotor with three different moments of inertia (MoI). Uniform rotation about the axis with the largest MoI corresponds to the lowest energy for given angular momentum (a.m.). For slightly larger energy, this axis executes harmonic oscillations about the space-fixed a.m. vector. The frequency of these oscillations is proportional to the rotational frequency of the rotor. For quantal systems these oscillations appear as equidistant excitations. They were first observed in molecular spectra, and theoretically analyzed in Ref. [2]. Bohr and Mottelson applied the concept to triaxial nuclei and introduced the name "wobbling" for the excitations. Figure 1 shows a triaxial rotor spectrum. With increasing spin I, the lowest excitations above the yrast states become more and more equidistant. This is the classical wobbling regime, which is characterized by an increasing wobbling frequency with I. Such wobbling spectra have rarely been observed in nuclei. The reason is that stable triaxial ground states are very uncommon. Figure 2 shows the best example identified so far.

The wobbling mode has been extensively studied for nuclei in the triaxial strongly deformed (TSD) region around $N = 94$, where a significant gap opens in the neutron levels at high spins for TSD shapes with $\varepsilon \approx 0.4$ and $\gamma \approx 20^\circ$ [5,6]. Wobbling bands have been identified in ^{161,163,165,167}Lu [3–8] and ^{167}Ta [9], which are built on configurations that contain an odd $i_{13/2}$ proton. As discussed in Ref. [10], the highly aligned odd proton plays a pivotal role in generating the wobbling excitations. The presence of an odd $i_{13/2}$ proton drives the nuclear shape toward large deformation thereby stabilizing a TSD shape. In addition it causes a general lowering of the wobbling frequency. This decrease made it possible to observe the one- and two-phonon wobbling excitations as individual bands, because it prevented them from being immersed among the numerous particle-hole excitations. A typical band spectrum of the odd-A wobblers is shown in Fig. 3. The wobbling frequency *decreases* with the spin I, in contrast to the simple wobblers shown in Figs. 1 and 2.

Following the discovery of the first wobbling structure in ^{163}Lu [3], the quasiparticle triaxial rotor (QTR) model was used to describe the wobbling mode, see Refs. [11–14]. Subsequent microscopic RPA calculations were able to reproduce experimental results, see Refs. [16–20]. In particular, the large ratios $B(E2)_{\rm con}/B(E2)_{\rm in}$ of interband to intraband $E2$ transitions could be described in both approaches. However, the calculated wobbling frequencies of the QTR model with the assumptions of Refs. [11,12] about the three MoI distinctly disagreed with experiment. Instead of the experimentally observed decrease, the wobbling frequency increased with the spin I (c.f. Fig. 3). The same was found for all the other cases

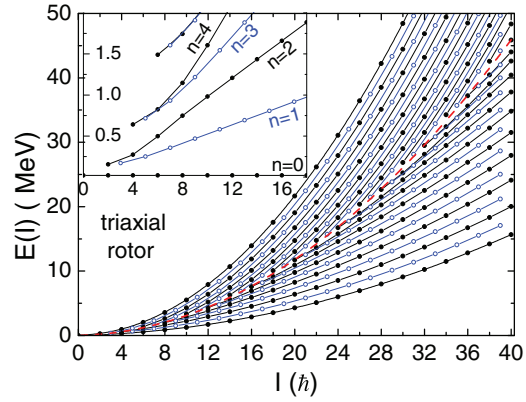

FIG. 1. (Color online) Rotational band structures calculated for the triaxial rotor Hamiltonian, Eq. (1). The inset shows a blow up of the energies of the lowest excited bands ($n = 1$–4) relative to the yrast line ($n = 0$). Full black dots belong to the states of signature $\alpha = 0$ and empty blue dots to signature $\alpha = 1$. The red dashed line displays the separatrix. The ratios of the rotational parameters are $A_1 = 6A_3$ and $A_2 = 3A_3$. The energies are scaled such that $E(2_1^+) = 0.1$ MeV.

*sfrauend@nd.edu

†doenau@hzdr.de

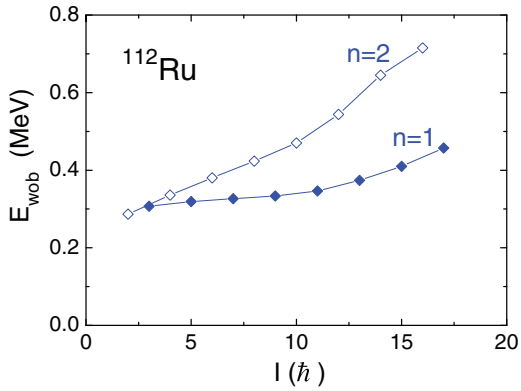

FIG. 2. (Color online) Experimental energies of the two lowest wobbling bands $n = 1$, 2 relative to the $n = 0$ yrast sequence (interpolated by a cubic spline) in ^{112}Ru. Data from [15].

from the TSD region (c.f. Ref. [10]). The RPA calculations, on the other hand, were able to reproduce the decrease of the wobbling frequency with I [16–20].

In this paper we readdress the wobbling mode in the framework of the QTR model. In Sec. II we carry out a semiclassical analysis of the QTR model assuming that the a.m. of the odd particle is rigidly aligned with one of the principal axes. This leads to the concept of a "transverse wobbler" and explains why its wobbling frequency decreases with I, in contrast to the "simple wobbler" usually considered. Staying within the frozen alignment approximation, simple analytical expressions for the energies and transition matrix elements are derived in Sec. III, which generalize the well known expressions for the simple wobbler. In Sec. IV we present detailed QTR calculations for ^{163}Lu and ^{135}Pr. We assume an arrangement of the MoI with respect to the principal axes that differs from the one in the previous QTR calculations [11–14]. We shall demonstrate that this "transverse" arrangement, which is consistent with microscopic calculations, results in both large inter-band to in-band $B(E2)$ ratios and a decrease of the wobbling frequency with spin. The results account well for the experimental findings.

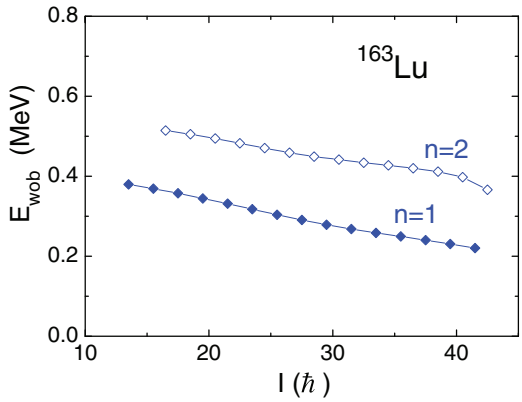

FIG. 3. (Color online) Experimental energies of the two lowest wobbling bands $n = 1$, 2 relative to the $\pi i_{13/2}$ $n = 0$ sequence (interpolated by a cubic spline) in ^{163}Lu. Data from [3].

II. SIMPLE, TRANSVERSE, AND LONGITUDINAL WOBBLERS

First, we review the semiclassical analysis of the familiar triaxial rotor, which we denote "simple rotor", to distinguish it from the cases to be discussed below. Bohr and Mottelson [21] discussed the rotational motion and pointed out the possible existence of wobbling excitations at high spin. They started from the Hamiltonian of a rigid triaxial rotor, which in the body fixed frame is given by

$$H = A_3\hat{J}_3^2 + A_1\hat{J}_1^2 + A_2\hat{J}_2^2, \tag{1}$$

where J_k are the a.m. components and A_k the rotational parameters with respect to the principal axes $k = 1,2,3$. Correspondingly, the moments of inertia $\mathcal{J}_k$ are given by the relation

$$\mathcal{J}_k = \frac{\hbar^2}{2A_k}. \tag{2}$$

The motion of the a.m. vector $\vec{J} = (J_1, J_2, J_3)$ can be conveniently visualized by considering the classical orbits of $\vec{J}$. These orbits are determined by the conservation of a.m.

$$J^2 = J_1^2 + J_2^2 + J_3^2 = I(I+1) \tag{3}$$

and energy

$$E = A_3J_3^2 + A_1J_1^2 + A_2J_2^2. \tag{4}$$

The classical orbit of $\vec{J}$ is the intersection of the a.m. sphere (3) with the energy ellipsoid (4). Let us assume that the axes are chosen such that $A_1 > A_2 > A_3$ or accordingly $\mathcal{J}_1 < \mathcal{J}_2 < \mathcal{J}_3$.

Figure 4 illustrates three types of orbits for a given a.m. value J, which is the radius of the a.m. sphere (3). We assume for the rotational parameters $A_1 = 6A_3$ and $A_2 = 3A_3$ and use the value A_3 as energy scale. The size of the energy ellipsoid increases with the energy E. The yrast line corresponds to touching between the surfaces (3) and (4) at the point $J_3 = J$. The nucleus rotates uniformly about the three-axis with the maximal MoI at the energy $E(J) = A_3J^2$. The upper panel shows an orbit just above the yrast line, which represents the harmonic wobbling motion as discussed by Bohr and Mottelson. The middle panel shows the orbit called separatrix. It has the energy of the unstable uniform rotation about the two-axis with the intermediate MoI. The frequency of this orbit is zero, because it takes infinitely long time to get to or to depart from the point of the labile equilibrium (uniform rotation about the two-axis). The orbits with larger energy than the one of the separatrix revolve the one-axis. The lower panel shows one example.

The wobbling excitations are small amplitude oscillations of the a.m. vector (J_1, J_2, J_3) about the three-axis of the largest MoI. Their energy is given by a harmonic spectrum of wobbling quanta [21]

$$H = A_3I(I+1) + \left(n + \tfrac{1}{2}\right)\hbar\omega_w, \tag{5}$$

where n is the number of wobbling quanta and the wobbling frequency $\hbar\omega_w$ is equal to

$$\hbar\omega_w = 2I\left[(A_1 - A_3)(A_2 - A_3)\right]^{1/2}. \tag{6}$$

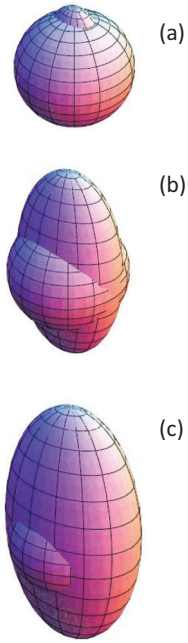

FIG. 4. (Color online) Classical a.m. sphere and energy ellipsoid for a simple triaxial rotor with the rotational parameters $A_1 = 6A_3$ and $A_2 = 3A_3$. The intersection line is the classical orbit of the a.m. vector relative to the body fixed frame. The three panels (a), (b), and (c) correspond to the orbits 1, 4, and 6 in Fig. 3.

Quantum mechanically one has to take into account the invariance of the rotor with respect to rotations by $\pi/2$ about its principal axes. It has the consequence that the states have a signature quantum number $\alpha = \mathrm{mod}(I,2) = I + \mathrm{even}$, which is fixed by the quantum number I of the a.m. In even-even nuclei the signature alternates between 0 and 1, starting with 0 for the yrast line. The first wobbling band ($n = 1$) has $\alpha = 1$. Above the separatrix, there are two classical orbits with the same energy, which revolve the positive and negative one-half axes. The corresponding quantal states are symmetric and antisymmetric combinations with signature 0 and 1, respectively. Figure 1 illustrates how the separatrix divides the quantal spectrum into the two types of states that correspond to classical orbits revolving the three- and one-axes. The inset shows how the harmonic wobbling mode emerges with increasing a.m. I.

In order to describe quantitatively the motion of $\vec{J}$ we introduce the canonical variables J_3 and ϕ,

$$J_1 = J_\perp \cos\phi, \quad J_2 = J_\perp \sin\phi, \quad J_\perp = \sqrt{J^2 - J_3^2}, \qquad (7)$$

where ϕ is the angle of the 1-axis with the projection of $\vec{J}$ onto the 1-2 plane. Inserting the definitions (7) into Eqs. (3),(4) gives the following equation for the orbits:

$$\phi(J_3) = \arcsin \sqrt{\frac{E - A_1(J^2 - J_3^2) - A_3 J_3^2}{(A_2 - A_1)(J^2 - J_3^2)}}. \qquad (8)$$

The phase space for the one-dimensional motion on the a.m. sphere is $-\pi \leqslant \phi \leqslant \pi$ and $-J \leqslant J_3 \leqslant J$. Figure 5 shows a series of orbits in the phase space. The stable minimum lies at

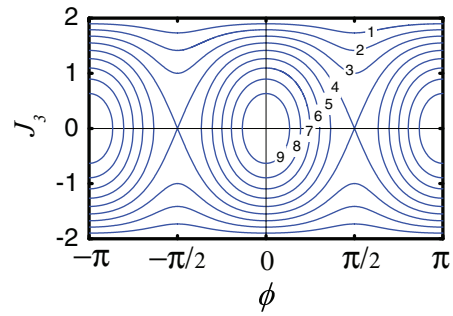

FIG. 5. (Color online) Classical orbits (blue lines) of the a.m. vector for a simple triaxial rotor with the rotational parameters $A_1 = 6A_3$ and $A_2 = 3A_3$. The a.m. is $J = 2$. The series of the orbits 1–9 corresponds to the energies $E = 6,8,\ldots,22$ in terms of the energy unit A_3.

the point where $J_3 = J$ (here equal $2\hbar$). Below, for a better comparison with the cases when a particle is present, we use the particle a.m. j as the unit for the total a.m. Orbit 1 corresponds to wobbling about the three-axis. Orbit 4 is the separatrix. Orbit 7 corresponds to wobbling about the one-axis. According to classical mechanics, the period of the orbit is $T = 2\pi dS/dE$, where S is the phase space area enclosed by the orbit. The orbits in Fig. 5 are calculated for an equidistant set of energies. As seen, the difference ΔS is maximal near the separatrix, which means there the period T has a maximum and the frequency $\omega = 2\pi/T$ has a minimum. In classical mechanics the energy increases continuously, and the frequency of the separatrix goes to zero, as mentioned above. In quantum mechanics the increase of the energy is discrete, such that $\Delta S = 2\pi\hbar$, i.e., the energy distance between adjacent levels has a minimum at the separatrix. For comparison we present in Fig. 1 the complete series of quantal band structures as calculated for the triaxial rotor with the same rotational parameters as in Fig. 5.

Now we discuss the wobbling excitations in odd-A triaxial nuclei. In order to account for the presence of a high-j odd quasiparticle, the triaxial rotor Hamiltonian must be replaced by the quasiparticle triaxial rotor (QTR) Hamiltonian

$$H = h_{dqp} + A_3(\hat{J}_3 - \hat{j}_3)^2 + A_1(\hat{J}_1 - \hat{j}_1)^2 + A_2(\hat{J}_2 - \hat{j}_2)^2, \qquad (9)$$

where $\hat{j}_k$ is the a.m. of the odd quasiparticle and $\hat{J}_k$ the total a.m. The term h_{dqp} describes the coupling of the odd quasiparticle to the triaxial core. Qualitatively, the coupling aligns the $\vec{j}$ of a high-j particle with the short (s) axis, because this orientation corresponds to maximal overlap between the density distribution of the particle and the triaxial core, which minimizes the attractive short range core-particle interaction. Likewise, the coupling aligns the $\vec{j}$ of a high-j hole with the long (l) axis, because this orientation corresponds to minimal overlap between the density distribution of the hole and the triaxial core, which minimizes the repulsive short range core-hole interaction. The coupling aligns the $\vec{j}$ of a quasiparticle from a half-filled high-j orbital with the medium (m) axis. These coupling schemes can be verified by microscopic calculation within the frame of the cranking model.

The coupling of the high-j quasiparticle to the triaxial rotor considerably modifies the motion of the a.m. vector $\vec{J}$ with respect to the body fixed frame. To carry out the semiclassical analysis we assume that the a.m. of the odd quasiparticle is rigidly aligned with one of the principal axes of the triaxial rotor. This "Frozen Alignment" (FA) approximation idealizes the above discussed tendency of the quasiparticle to align its a.m. with one of the principal axes according to its particle-hole character. In the following we assume that the alignment is along the three-axis. Again, the motion of the a.m. vector is visualized by the classical orbits of $\vec{J}$, which are determined by the conservation of a.m. and the energy. The classical orbits of $\vec{J}$ are the intersection of the a.m. sphere (3) with the shifted energy ellipsoid

$$E = A_3(J_3 - j)^2 + A_1 J_1^2 + A_2 J_2^2. \quad (10)$$

Accordingly, in Eq. (8) for the orbit $\phi(J_3)$ the term $A_3 J_3^2$ has to be replaced by the shifted term $A_3(J_3 - j)^2$.

As discussed above, the triaxial shape of the rotor determines the orientation of quasiparticle with respect to its principal axes. However, it also determines the ratios between the three MoI, which are of the hydrodynamic type: The MoI of the medium (m) axis is always the largest. This can be inferred from a simple argument that holds for both the hydrodynamic and quantal systems. The MoI is zero for rotation about a symmetry axis and increases with the deviation from axial symmetry of the axis. The triaxial shape deviates most strongly from axial symmetry with respect to the m-axis, which results in the largest MoI. Microscopic calculation based on the cranking model typically give the order $\mathcal{J}_l < \mathcal{J}_s < \mathcal{J}_m$ using again the notation l,s and m for the long, short, and medium axes, respectively. The microscopic ratios deviate from the hydrodynamic ones. In particular, for $\gamma = 30^\circ$ one still has $\mathcal{J}_l < \mathcal{J}_s < \mathcal{J}_m$ in contrast to the hydrodynamic ratios $\mathcal{J}_l = \mathcal{J}_s < \mathcal{J}_m$ (see Table I below).

One must distinguish between the quasiparticle a.m. vector $\vec{j}$ being aligned with the m-axis with the largest MoI, which we refer to as the *longitudinal* case, and the vector $\vec{j}$ being perpendicular to the m-axis, which we refer to as the *transverse* case. A quasiparticle with predominantly particle character, which emerges from the bottom of a deformed j shell, aligns its $\vec{j}$ with the s-axis. It combines with the triaxial rotor (TR) to a transverse QTR system. A quasiparticle with predominantly hole character, which emerges from the top of a deformed j shell, aligns its $\vec{j}$ with the l-axis. It couples with the TR to a transverse QTR too. A quasiparticle, which emerges from the middle of the j shell and tends to align with the m-axis, couples with the TR to a longitudinal QTR. The Coriolis force tends to realign $\vec{j}$ from the s- or l- axes toward the m-axis. It may overcome the coupling to the deformed potential, resulting in a change from the transverse to the longitudinal mode.

TABLE I. Deformation parameters and moments of inertia (in $\hbar^2$/MeV) used in the QTR and HFA calculations. The letters m,s,l denote the medium, short, long axes of the triaxial potential and charge distribution.

Nucleus	ε	γ(deg)	Model	$\mathcal{J}_m$	$\mathcal{J}_s$	$\mathcal{J}_l$
^{135}Pr	0.16	26	fit	21	13	4
	0.16	26	hydrodyn	20	6	4
	0.16	26	cranking	17	7	3
^{163}Lu	0.4	20	fit	64	56	13
	0.4	20	hydrodyn	68	29	8
	0.4	20	cranking	59	51	13

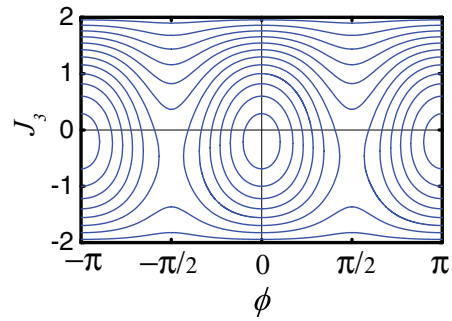

FIG. 6. (Color online) Classical orbits (blue lines) of the a.m. vector for a longitudinal triaxial rotor with a high-j particle. The rotational parameters are $A_1 = 6A_3$ and $A_2 = 3A_3$. The a.m. is $J = 2$ in units of the particle a.m. j. The topmost orbital has $E = 2$ in terms of the energy unit $A_3 j^2$ and beneath the energy is increasing in steps of 2.

The longitudinal QTR is similar to the simple rotor, only that the energy ellipsoid, Eq. (10), is shifted upwards by j. The yrast line corresponds to uniform rotation about the three-axis and the lowest excited states represent wobbling about this axis as shown in the upper panel of Fig. 4. The orbits in phase space are shown in Fig. 6. The wobbling bands in this odd-A case have alternating signature $\alpha = \pm \mod(j,2)$, starting with $\alpha = \mod(J,2)$ at the yrast line. The wobbling frequency increases with a.m.. We mention that the "reversed arrangement" (as compared to the hydrodynamic one) of the MoI used in Refs. [11,12] for the description of wobbling bands in the Lu isotopes corresponds to a longitudinal QTR. This arrangement is inconsistent with above discussed natural order $\mathcal{J}_l < \mathcal{J}_s < \mathcal{J}_m$, because the odd $i_{13/2}$ quasiproton has particle character and as such aligns its $\vec{j}$ with the s-axis, to which the maximal MoI is assigned.

For the analysis of the transverse QTP, we assume the quasiparticle to be particle-like, i.e., the three-axis is the s-axis. Further, we assign the two-axis to the m-axis with the largest MoI and the one-axis to the l-axis with the smallest MoI. (The axes 2 and 3 are exchanged compared to the discussion of the simple TR and the longitudinal QTR.) The pertinent figures are generated with the rotational parameters $A_1 = 6A_2$, $A_2 = A_2$, and $A_3 = 3A_2$. As illustrated by Fig. 7, the resulting yrast line consists of two pieces. At low a.m. it corresponds to rotation about the three-axis. The energy ellipsoid touches the a.m. sphere at the point $J_3 = J$ on the three-axis and the yrast energy is $E = A_3(J - j)^2$. The low energy orbits above yrast represent wobbling about the three-axis. Figure 8 displays the intersection line of the lowest orbit in Fig. 10, which shows the orbits in phase space. At the critical a.m. $J_c = jA_3/(A_3 - A_2)$ the rotational axis of the yrast line flips to the direction of

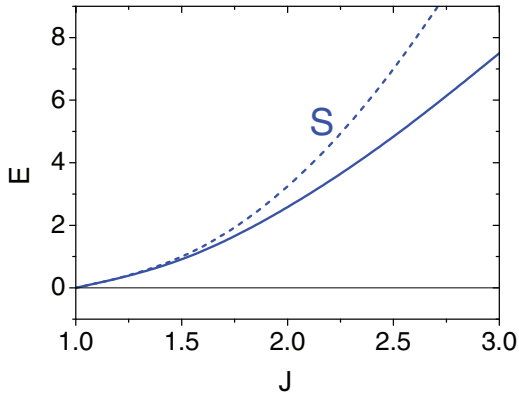

FIG. 7. (Color online) Energy E of the yrast line and the separatrix (S) for the transverse rotor with the rotational parameters $A_1 = 6A_2$ and $A_3 = 3A_2$. The unit of the a.m. J is j, and the energy unit is $A_2 j^2$.

the point $J_1 = 0$, $J_2 = \sqrt{J^2 - J_c^2}$, $J_3 = J_c$, where the energy ellipsoid touches the a.m. sphere from inside. This means, the axis of uniform rotation is tilted into the s-m plane. Quantum mechanically, rotation about such a tilted axis corresponds to merging of the two signatures into a $\Delta I = 1$ band. The upper panel of Fig. 9 displays the intersection of the energy ellipsoid with a.m. sphere for a slightly higher energy, which is the first orbit enclosing the touch point ($\phi = \pi/2$, $J_3 = 3/2j$) in Fig. 11.

The separatrix, which is illustrated in the middle panel of Fig. 9, lies at $E = A_3(J - j)^2$. Above the separatrix the orbits revolve the three-axis as shown in the lower panel of Fig. 9.

For $J < J_c$ the yrast line is $E = A_3(J - j)^2$. It continues as separatrix for $J > J_c$. As discussed above for the simple rotor, the classical frequency of the separatrix is zero. Analogously for the transverse QTR the frequency of the small-amplitude wobbling goes to zero at $J = J_c$, where uniform rotation about the three-axis becomes unstable, and the new branch of the yrast line starts.

Quantum mechanically, the yrast states have signature $\alpha = \mathrm{mod}(j,2)$ for $J < J_c$, and the first wobbling state has opposite signature $-\alpha$. It encloses the fixed area $2\pi\hbar$ in phase space, which means its energy decreases with J. It merges with the yrast line, which becomes a $\Delta I = 1$ sequence for $J > J_c$. In case of the longitudinal rotor, there is no bifurcation of the yrast line, which is reflected by a continuous increase of the wobbling frequency with J.

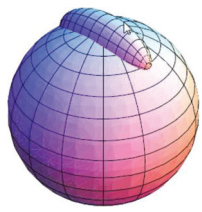

FIG. 8. (Color online) Angular momentum sphere and energy ellipsoid for a transverse QTR with the rotational parameters $A_1 = 6A_2$ and $A_3 = 3A_2$. The intersection line is the classical orbit of the a.m. vector relative to the body fixed frame. This line corresponds to the lowest energy orbit in Fig. 10.

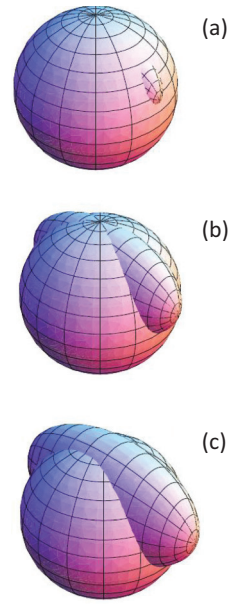

FIG. 9. (Color online) Angular momentum sphere and energy ellipsoid for a transverse QTR with the rotational parameters $A_1 = 6A_2$ and $A_3 = 3A_2$. The intersection line is the classical orbit of the a.m. vector relative to the body fixed frame. The three panels (a), (b), and (c) correspond to the orbits with the smallest energy, the separatrix, and the next orbit with higher energy, respectively, in accordance with the orbits shown in Fig. 11.

III. HARMONIC WOBBLING MODEL

Now we consider small amplitude wobbling vibrations about the three-axis. We retain the FA approximation, i.e., the a.m. of the odd quasiparticle is assumed to be firmly aligned with the three-axis and can be considered as a number. Then

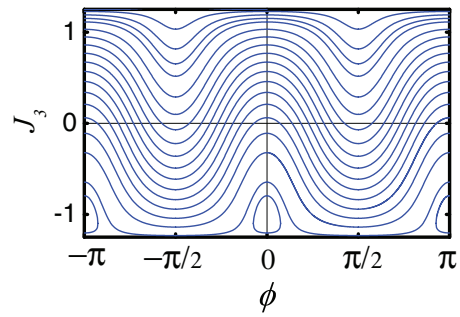

FIG. 10. (Color online) Classical orbits (blue lines) of the a.m. vector for a transverse triaxial rotor with the rotational parameters $A_1 = 6A_2$ and $A_3 = 3A_2$. The a.m. is $J = 1.25j$ being below the critical a.m. J_c. The a.m. unit is j. The energy increases from the top to the bottom. The energy difference between the orbits is 1, where the energy unit is $A_2 j^2$. The separatrix is located in the lower part of the figure right above the closed orbits at $\phi = 0, \pm\pi$.

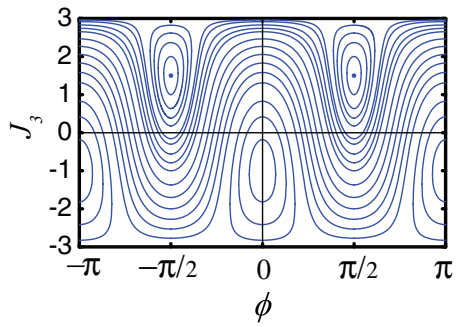

FIG. 11. (Color online) Classical orbits (blue lines) of the a.m. vector for a transverse triaxial rotor with the rotational parameters $A_1 = 6A_2$ and $A_3 = 3A_2$. The a.m. is $J = 3$ which is above the critical a.m. J_c. The a.m. unit is j. The energy difference between the orbits is 4, where the energy unit is $A_2 j^2$. The dot indicates the yrast "orbit", from where the energy increases.

the QTR Hamiltonian becomes

$$H = A_3(\hat{J}_3 - j)^2 + A_1\hat{J}_1^2 + A_2\hat{J}_2^2, \tag{11}$$

where j is a number. We use the second-order expansion

$$\hat{J}_3 = \sqrt{J^2 - \hat{J}_1^2 - \hat{J}_2^2} \approx J - \frac{1}{2}\left(\frac{\hat{J}_1^2}{J} + \frac{\hat{J}_2^2}{J}\right), \tag{12}$$

where $J = \sqrt{I(I+1)}$. The Hamiltonian becomes in harmonic FA (HFA) approximation

$$H = A_3(J - j)^2 + (A_1 - \bar{A}_3)\hat{J}_1^2 + (A_2 - \bar{A}_3)\hat{J}_2^2, \tag{13}$$

where

$$\bar{A}_3 = A_3(J) = A_3\left(1 - \frac{j}{J}\right). \tag{14}$$

This Hamiltonian has the form of the simple TR Hamiltonian, except that A_3 is replaced by the J-dependent rotational parameter $\bar{A}_3(J) = A_3(1 - j/J)$. Therefore, one can carry over the expressions given by Bohr and Mottelson [21] replacing A_3 by $\bar{A}_3(J)$.[1] The wobbling frequency becomes

$$\hbar\omega_w = 2J[(A_1 - \bar{A}_3(J))(A_2 - \bar{A}_3(J))]^{1/2}. \tag{15}$$

Correspondingly, the $E2$-transition probabilities are [21]

$$B(E2,n,I \to n,I \pm 2) = \frac{5}{16\pi}e^2Q_2^2, \tag{16}$$

$$B(E2,n,I \to n-1,I-1) = \frac{5}{16\pi}e^2\frac{n}{J}(\sqrt{3}Q_0x - \sqrt{2}Q_2y)^2, \tag{17}$$

$$B(E2,n,I \to n+1,I+1) = \frac{5}{16\pi}e^2\frac{n+1}{J}(\sqrt{3}Q_0y - \sqrt{2}Q_2x)^2, \tag{18}$$

where

$$\begin{bmatrix} x \\ y \end{bmatrix} = \begin{pmatrix} 1 \\ -\mathrm{sign}(\beta) \end{pmatrix}\left[\frac{1}{2}\left(\frac{\alpha}{\hbar\omega_w} \pm 1\right)\right]^{1/2}, \tag{19}$$

$$\alpha = (A_1 + A_2 - 2\bar{A}_3(J))J, \quad \beta = (A_1 - A_2)J \tag{20}$$

and Q_0 and Q_2 are the quadrupole moments of the triaxial charge density relative to the three-axis. The transition probabilities $B(M1)$ can be derived analogously to the $B(E2)$ in Ref. [21] by assuming that the aligned quasiparticle generates a magnetic moment component $\mu_3 = (g_j - g_R)j$. One finds

$$B(M1,n,I \to n-1,I-1) = \frac{3}{4\pi}\frac{n}{J}[j(g_j - g_R)x]^2, \tag{21}$$

$$B(M1,n,I \to n+1,I+1) = \frac{3}{4\pi}\frac{n+1}{J}[j(g_j - g_R)y]^2. \tag{22}$$

The harmonic approximation is valid as long as $J_1^2 + J_2^2 \ll J^2$. For the first wobbling excitation this leads to the condition [21]

$$\frac{3(A_1 + A_2 - 2\bar{A}_3)}{2(A_1 - \bar{A}_3)^{1/2}(A_2 - \bar{A}_3)^{1/2}} \ll J. \tag{23}$$

Let us discuss the wobbling energy, Eq. (15), in more detail. It can be rewritten as

$$\hbar\omega_w = \frac{j}{\mathcal{J}_3}\left[\left(1 + \frac{J}{j}\left(\frac{\mathcal{J}_3}{\mathcal{J}_1} - 1\right)\right)\left(1 + \frac{J}{j}\left(\frac{\mathcal{J}_3}{\mathcal{J}_2} - 1\right)\right)\right]^{1/2}. \tag{24}$$

For the longitudinal QTR, the relation $\mathcal{J}_3 > \mathcal{J}_1, \mathcal{J}_2$ holds. Both bracketed terms in Eq. (15) are positive, and the wobbling frequency increases with a.m.

In case of the transverse QTR with an odd particle one has $\mathcal{J}_3 > \mathcal{J}_1$ but $\mathcal{J}_3 < \mathcal{J}_2$. Then, the factor $1 + J(\mathcal{J}_3/\mathcal{J}_2 - 1)/j$ in Eq. (24) decreases with J, and the wobbling energy will also decrease for sufficiently large J. It reaches zero at $J_c = j\mathcal{J}_2/(\mathcal{J}_2 - \mathcal{J}_3)$, which is the previously discussed critical a.m. where the separatrix bifurcates from the yrast line. There the yrast and the wobbling bands will merge into a single $\Delta I = 1$ sequence, reflecting the fact that the rotational axis is tilted into the s-m plane. Figures 13 and 14 show examples. The initial increase of the wobbling frequency in the case of ^{163}Lu is caused by the factor $1 + J(\mathcal{J}_3/\mathcal{J}_1 - 1)/j$ in Eq. (24), which increases with J. It is characteristic for a situation when $\mathcal{J}_m$ is only slightly larger than $\mathcal{J}_s$ but both are much larger than $\mathcal{J}_l$.

The transverse QTR with an odd hole has typically $\mathcal{J}_3 < \mathcal{J}_1, \mathcal{J}_2$. Then, both factors $1 + J(\mathcal{J}_3/\mathcal{J}_2 - 1)/j$ and $1 + J(\mathcal{J}_3/\mathcal{J}_1 - 1)/j$ in Eq. (24) decrease with J, and the wobbling energy will always decrease with J.

The prerequisite (23) for the small amplitude approximation is violated near the instability of the transverse QTR, which means that HFA cannot be applied there. The assumption of frozen alignment will become invalid at a certain a.m., when the inertial forces overcome the coupling of the odd quasiparticle to the TR. Then the quasiparticle $\vec{j}$ will realign with the m-axis and the QTR will change from the transverse

[1] Reference [21] uses the arrangement $\mathcal{J}_1 > \mathcal{J}_2 > \mathcal{J}_3$, which differs from the arrangement in this paper. In taking over the expression one has to relabel the axes accordingly.

to the longitudinal mode. Nevertheless, the set of equations (15)–(21) obtained from the HFA model provides an easily manageable tool for investigating the properties of the QTR system. In particular, it is the analytic form of these relations which allows us to qualitatively interpret the results of experiment and more sophisticated calculations.

The previous studies of the Lu isotopes with the QTR model [11–14] were based on the assumption $A_3 < A_1, A_2$ ($\mathcal{J}_3 > \mathcal{J}_1, \mathcal{J}_2$) together with the quasiparticle alignment $\vec{j}$ along the three-axis, which in our terminology is the longitudinal wobbler. Thus, the energies of the excited wobbling bands relative to the lowest $\pi i_{13/2}$ band must increase with spin, which is the opposite trend observed in Fig. 3. We suggest that the observed wobbling excitations are of the transverse type, i.e., we adopt the arrangement $A_2 < A_3 < A_1$, which corresponds to the natural order $\mathcal{J}_m > \mathcal{J}_s > \mathcal{J}_l$ obtained in microscopic cranking calculations.

Tanabe and Sugawara-Tanabe [13,14] considered a less restrictive approximation to the QTR than HFA. It assumes that the odd particle is not rigidly fixed to the core. Its a.m. may execute small amplitude oscillations. They find a moderate coupling between the two oscillators, such that the lowest states may be classified as being predominantly a wobbling mode of the core or a vibrational excitation of the odd particle. Our discussion above concerns only the first type, the wobbling modes. Naturally, their approach better reproduces the exact QTR results than our HFA, which however comes at the expense of rather complicated expressions.

IV. QTR CALCULATIONS

A. Model parameters

Below we present the results of our calculations for the transverse wobblers ^{135}Pr and ^{163}Lu obtained by means of the QTR model. The results will be compared with with the HFA and the experiment. Our QTR calculations have been carried out by using the core-quasiparticle-coupling (CQM) formalism [23], which at variance with usual QTR Hamiltonian (9) is formulated in the laboratory frame of reference. The CQM Hamiltonian is given by

$$H = h_{sqp} + H_{\rm core} - \kappa \sum_{\mu} q^*_{\mu} Q_{\mu}, \qquad (25)$$

where h_{sqp} accounts for the presence of the spherical potential and the monopole pair field, and $H_{\rm core}$ describes the collective motion of the TR core as given by Eq. (1). The third term realizes the quadrupole-quadrupole coupling between quasiparticles and the core. For completeness, we show in the Appendix the equivalence of the CQM Hamiltonian (25) with the more familiar QTR Hamiltonian (9).

The Hamiltonian (25) is diagonalized within the KKDF framework, which combines the equations of motion of Kerman and Klein [24] with the projection technique of Dönau and Frauendorf [23]. The CQM proved to be a flexible method for coupling any model for the collective quadrupole mode of the even-even core with one quasiparticle to describe the spectral properties of the considered odd-A nucleus. In our case the cores of ^{135}Pr and ^{163}Lu are assumed to be triaxial rotors, and the results of our CQM are equivalent with the ones of a QTR calculation in a deformed basis, as, e.g., the calculations in Refs. [4,11,12]. In a first step, the simple TR problem is numerically solved, which provides the matrices $H_{\rm core}$ and Q_{μ}. Since we consider the coupling to pure $h_{11/2}$ and $i_{13/2}$ quasiprotons, respectively, the term h_{sqp} contains only the gap parameter Δ and the difference $\varepsilon - \lambda$ between the spherical single particle level ε and the chemical potential λ. In the considered nuclides we assume the odd quasiparticles to be totally particle-like by taking $\varepsilon - \lambda = 6$ and 10 MeV in ^{135}Pr and ^{163}Lu, respectively. The chosen value $\Delta = 1$ MeV of the gap is then unessential for the results of our calculations.

The input parameters needed for specifying the properties of the rigid triaxial rotor core are summarized in Table I. The deformation parameters ε and γ are taken from the energy minima of the total Routhian surfaces calculated with the micro-macro method. Actually, for ^{163}Lu we extracted the deformations from Fig. 1 in Ref. [4]. The deformations of ^{135}Pr are identified with the minimum values in the total Routhian surface shown in Fig. 12, which we calculated with the tilted axis cranking (tac) code [22]. As discussed in Ref. [20], the deformation parameters as well as the MoI obtained from cranking mean field calculations moderately depend on spin. This dependence is neglected, and the parameters in Table I are to be considered as average values. We are studying the consequences of the spin dependence of the core parameters in the frame work of the QCM and will report the results in a forthcoming paper. We investigated three parameter sets for the MoI. The first set was obtained by freely adjusting of the MoI to achieve optimal agreement with the experimental energies of the wobbling bands. For the second set we adopted to ratios of the MoI obtained by means of the tac model [22]. For the third set we used the calculated triaxiality γ in order to determine the ratios between the MoI according to hydrodynamic model $\mathcal{J}_{k=1,2,3} = \mathcal{J}_o \sin^2(\gamma - 2\pi k/3)$. For both the second and third set the scaling factor $\mathcal{J}_o$ for the MoI was determined recursively by adapting $\mathcal{J}_o$ to the energies of the $n = 0$ zero-phonon band of the wobbler. The results of the

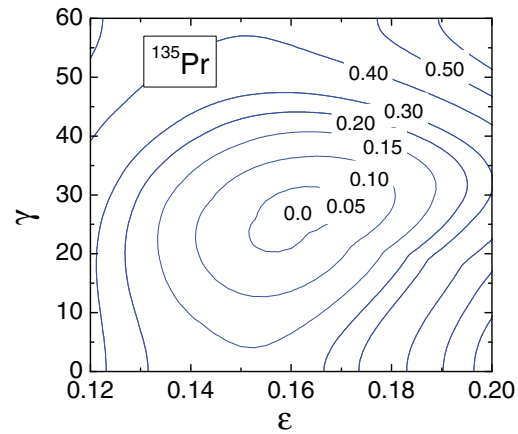

FIG. 12. (Color online) Potential energy surface $E(\varepsilon,\gamma)$ of ^{135}Pr calculated with the Strutinsky micro-macro method using the tilted axis cranking model [22]. The energies attached to the equipotential lines are in MeV.

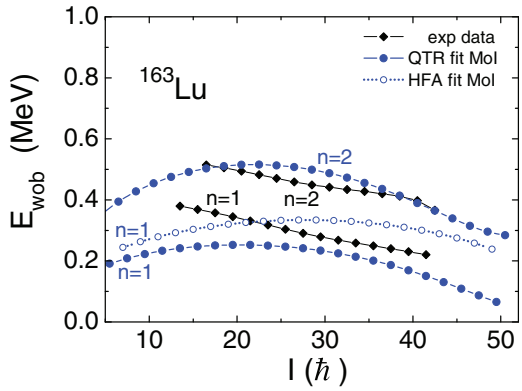

FIG. 13. (Color online) Excitation energies of the $n = 1$ and $n = 2$ wobbling bands in ^{163}Lu. Solid blue lines and full dots: QTR calculation with fitted MoI. Dotted blue line and open dots: HFA calculation for the $n = 1$ band with fitted MoI. Black lines and full diamonds: Experimental data.

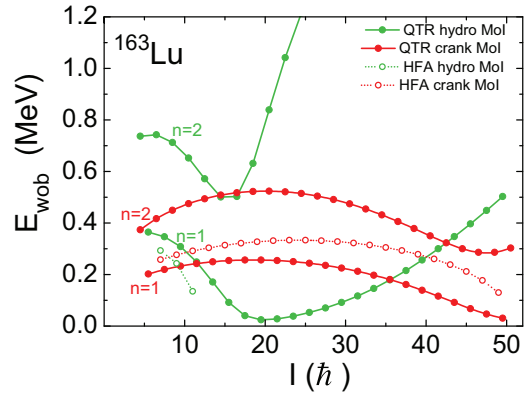

FIG. 15. (Color online) Excitation energies of the $n = 1$ and $n = 2$ wobbling bands in ^{163}Lu. Solid red lines and full dots: QTR with cranking MoI, solid green lines and full dots: QTR with hydrodynamic MoI. Dotted lines and open dots: HFA with cranking and hydrodynamic MoI, respectively.

QTR calculations are presented in Figs. 13–19 and Table II. They are compared with the available experimental data and in some cases with the HFA.

B. Quality of the HFA

Figures 13, 17, and 19 compare QTR energies and transition probabilities for ^{163}Lu with the HFA approximation. The HFA reproduces the full QTR in a fair way. Figure 14 shows that the differences between the QTR and HFA are more significant for ^{135}Pr. This is expected, because the $\vec{j}$ of the odd proton is less firmly aligned with the s-axis in ^{135}Pr, which has a small deformation ($\varepsilon = 0.16$), compared to ^{163}Lu, which has a much larger deformation ($\varepsilon = 0.4$). Although the scale of the wobbling frequency in ^{135}Pr is substantially overestimated, the instability of the transverse wobbler in HFA lies close to the minimum of the wobbling frequency of the QTR calculation. The merging of the zero- and one-phonon bands into a $\Delta I = 1$ band after the HFA instability does not occur for the QTR calculation. Instead, the relatively weakly coupled proton realigns with the m-axis, and the wobbler changes from the transverse into the longitudinal mode. Figure 15 also shows the QTR calculation for ^{163}Lu using the hydrodynamic ratios between the MoI. As expected from Eq. (24), the larger ratio of $\mathcal{J}_s/\mathcal{J}_m = 2.34$ (as compared to 1.14 for the cranking ratios) down shifts the instability to $I = 20$. In the spin range $20 < I < 30$ the two signature sequences are very close in energy. The larger deformation of ^{163}Lu delays the realignment of the odd proton to higher a.m., whereas in the less deformed nuclide ^{135}Pr it occurs already at the instability. For $n = 1$, the HFA for the ratio $B(E2, I \to I-1)/B(E2, I \to I-2)$ somewhat overestimates the scale of the QTR values but nicely follows the down trend with I. For $n = 2$ the HFA estimate (two times the $n = 1$ value) largely overestimates the QTR values (see Fig. 17).

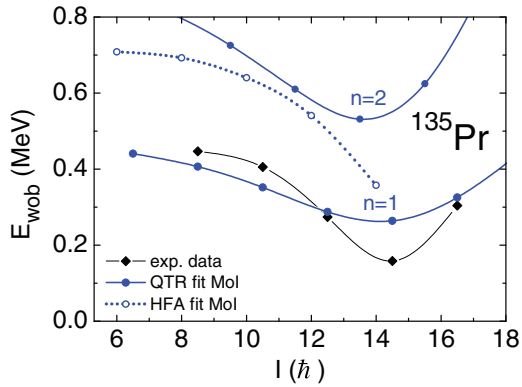

FIG. 14. (Color online) Excitation energies of the $n = 1$ and $n = 2$ wobbling bands in ^{135}Pr. Solid blue lines and full dots: QTR calculation with fitted MoI. Dotted blue lines and open dots: HFA calculation with fitted MoI. Black line and full diamonds: Experimental data.

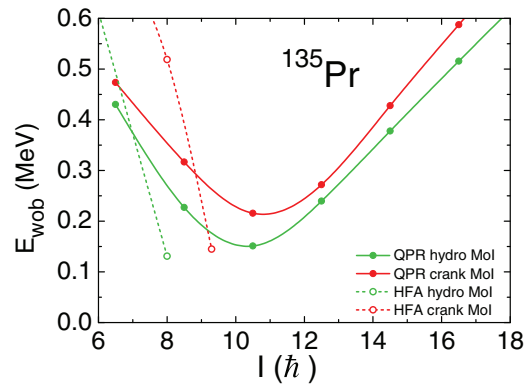

FIG. 16. (Color online) Excitation energies of the wobbling band in ^{135}Pr. Solid red lines and full dots: QTR with cranking MoI, solid green lines and full dots: QTR with hydrodynamic MoI. Dashed lines and open dots: HFA with cranking and hydrodynamic MoI, respectively.

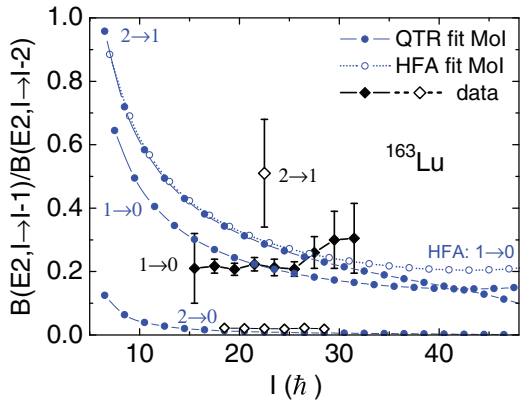

FIG. 17. (Color online) $B(E2)$ ratios of the connecting to in-band transitions $n = 1,2 \rightarrow n = 1,0$ of the wobbling bands in ^{163}Lu. Solid blue line and full dots: QTR with fitted moments of inertia, dashed blue line and open dots: HFA with fitted moments of inertia. Black: Experimental data. The numbers indicate the actual transition $n \rightarrow n'$.

C. Comparison with experiment

The decreasing experimental wobbling frequency classifies both ^{163}Lu and ^{135}Pr as transverse wobblers. ^{163}Lu has a quite long band with an almost linear fall-off of the frequency. The sequence in ^{135}Pr is short, and the wobbling frequency turns up at its end. As already discussed, the difference is the consequence of the different deformation ε. The considered bands in ^{163}Lu are based on a highly deformed shape with $\varepsilon = 0.4$. The bands in ^{135}Pr belong to a weakly deformed shape with $\varepsilon = 0.16$. This results in a factor of three between the size of the moments of inertia and consequently in the scale of the a.m. Accordingly, one expects the strongly deformed ^{163}Lu to be a better case than the less deformed ^{135}Pr for describing the wobbling motion in terms of a rigid triaxial rotor.

The general trend of the decreasing wobbling frequency is reproduced in our calculations with the QTR and the HFA model. According to the HFA approximation, the wobbling band terminates at the critical spin value where the a.m. of the

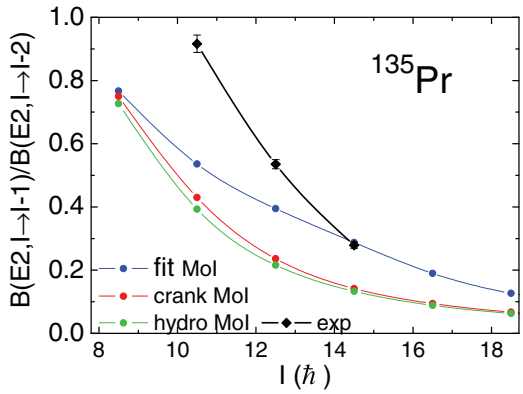

FIG. 18. (Color online) $B(E2)$ ratios of the connecting to in-band transitions $n = 1 \rightarrow n = 0$ of the wobbling band in ^{135}Pr. Solid blue line: QTR calculated with fitted moments of inertia, red (green) line: with cranking (hydrodynamic) moments of inertia. Black: Experimental data (cf. Table II).

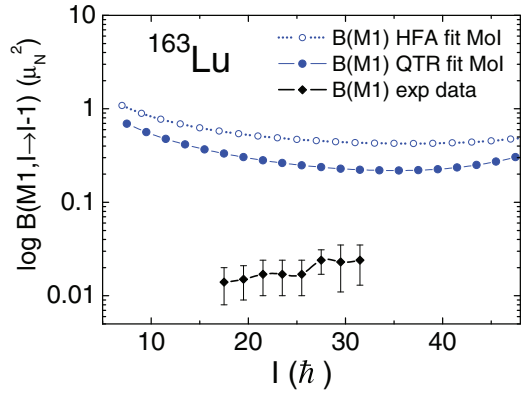

FIG. 19. (Color online) $B(M1, I \rightarrow I-1)$ of the connecting transitions $n = 1 \rightarrow n = 0$ of the wobbling band in ^{163}Lu. Solid blue line and full dots: QTR with fitted moments of inertia, dashed blue line and open dots: HFA with fitted moments of inertia. Black: Experimental data.

triaxial rotor changes from principal axis to tilted axis rotation. One notices that this change of the a.m. coupling is born out by the QTR calculations. The observed kink of the band in ^{135}Pr at $I = 29/2$ can be related to the transition. In ^{163}Lu the predicted end of transverse wobbling regime at $I = 103/2$ has not been reached at $I = 83/2$ in experiment.

Figures 13, 15–17 compare the excitation energies of the wobbling bands in ^{163}Lu and ^{135}Pr obtained from QTR model with cranking and hydrodynamic MoI with the ones obtained with the MoI adjusted to best agreement with experiment (cf. Table I). In the case of ^{163}Lu, the microscopically calculated cranking MoI are very close to the fitted values and give a satisfactory agreement with the experimental data. The cranking model works well in the high spin region of well deformed nuclei. In contrast, the hydrodynamic MoI lead to a much too early instability at $I = 20$, where the wobbling frequency starts increasing again. As discussed in Sec. IV B,

TABLE II. B values and ratios $r_{M1} = B(M1)_{con}/B(E2)_{in}$ and $r_{E2} = B(E2)_{con}/B(E2)_{in}$ of the wobbling states in ^{135}Pr. The suffices *in* and *con* refer to the in-band $\Delta I = 2$ and $\Delta I = 1$ transitions that connect the bands, respectively. The B values and the calculated ratios r^{cal} result from our QTR calculations with the fitted MoI. The tentative experimental ratios r^{exp} were made available prior publication by Matta *et al.* [26].

Spin I	$B(E2)^{cal}_{in}$	$B(E2)^{cal}_{con}$	$B(M1)^{cal}_{con}$	
17/2	0.637	0.488	0.243	
21/2	0.744	0.399	0.187	
25/2	0.838	0.331	0.167	
29/2	0.930	0.267	0.167	
33/2	1.023	0.194	0.155	
Spin I	r^{cal}_{M1}	r^{exp}_{M1}	r^{cal}_{E2}	r^{exp}_{E2}
17/2	0.381	–	0.767	–
21/2	0.252	0.130 ± 0.011	0.536	0.92 ± 0.03
25/2	0.199	0.021 ± 0.004	0.395	0.535 ± 0.01
29/2	0.180	0.010 ± 0.002	0.288	0.28 ± 0.01
33/2	0.151	–	0.190	–

this is the consequence of the large ratio of $\mathcal{J}_m/\mathcal{J}_s = 2.34$. In ^{135}Pr the calculations with the cranking MoI and with the hydrodynamic MoI give a too small critical spin (minimum), which reflects the large ratio $\mathcal{J}_m/\mathcal{J}_s = 2.4$ and 3.3, respectively. The ratio 1.6 between the fitted MoI places the minimum at the right value of I. The QTR reproduces the observed increase of the wobbling frequency above $I = 14$. It is caused by the reorientation of the odd proton from being aligned with the short axis toward the medium axis, which corresponds to a transition from transverse to longitudinal wobbling (c.f. discussion in Sec. IV B). Experimentally, the minimum is more pronounced than in the QTR calculations. One reason is that the experimental function $I(\omega)$ of the yrast band shows a back bend at $I = 14$, which is not accounted for by the TR core of the QTR.

The two-phonon ($n = 2$) wobbling band has been identified in ^{163}Lu, which the QTR calculation places close at the observed excitation energy. The light convex bending of both the one- and two-phonon bands obtained by the QTR calculation is not seen in the experimental sequences of ^{163}Lu. No candidate for a two-phonon has been found in ^{135}Pr.

As can be seen in Fig. 13, the QTR energy of the two-phonon is about twice the energy of the one-phonon bands for $I < 30$, whereas this ratio is considerably lower in the experimental band. So far, we have no explanation for this discrepancy. For larger values of I, the QTR ratio increases. This is explained as follows. The one-phonon band has opposite signature than the zero-phonon band. Because of their different symmetry the two bands may approach and even cross. The two-phonon band has the same signature as the zero-phonon band, and the two bands can mix and repel each other. The onset of the repulsion is seen around $I = 50$. The experiment also shows an increasing of the ratio of the two- and one-phonon energies.

The ratios $B(E2, I \to I-1)/B(E2, I \to I-2)$ for the transitions connecting the bands (con) and the in-band transitions (in) in ^{163}Lu are shown in Fig. 17. The QTR calculations reproduce the strong connecting $E2$ transitions observed in experiment, which are the evidence for the collective nature of wobbling excitations. The calculated ratios 0.3–0.2 are in accordance with experiment [25]. However, the experimental ratio is weakly increasing within the observed spin interval $I = 31/2 - 63/2$, whereas the QTR calculation gives a slightly decreasing ratio. The HFA shows the same tendency as QTR. The measured ratio $B(E2, I \to I-1)/B(E2, I \to I-2) = 0.5 \pm 0.15$ at $I = 45/2$ is about twice as large as the ratio of the corresponding $n = 1$ to $n = 0$ transition which supports the two-phonon nature of the upper band. In the QTR calculation the corresponding ratio between $n = 2$ and $n = 1$ out-of-band transitions is with about 1.3 too low for a clear two-phonon structure of the calculated $n = 2$ band.

The ratios $B(E2, I \to I-1)/B(E2, I \to I-2)$ shown in Fig. 18 for ^{135}Pr are obtained with the QTR model using the three parameter sets for the MoI in Table I. The ratios slope down with increasing spin. The calculation with the fitted moments of inertia predicts the strongest interband $E2$ transitions, corresponding to a ratio of 0.5–0.3 within the spin interval $I = 10$–14. The tentative experimental ratios [26] are larger and decrease more rapidly.

Figure 19 displays the $B(M1)$ values of the connecting transitions $I \to I-1$ of the one-phonon wobbling band in ^{163}Lu. The measurements [25] found very small $M1$ admixtures to the nonstretched $E2$ transitions. The QTR and the HFA calculation also predict only a weak $M1$ admixture. However, the relatively flat curve with a minimum of about $0.2\ \mu_N^2$ overestimates the measured $B(M1)$ values by more than a factor of 10. The QTR calculations with the cranking and hydrodynamic moments of inertia gave similar $B(M1)$ values. The QTR calculations for the wobbling band in ^{135}Pr predict $B(M1, I \to I-1) \approx 0.2\ \mu_N^2$ for each of the three sets of MoI. The recent experiment by Matta *et al.* [26] provided the tentative ratios $r_{M1} = B(M1)_{\rm out}/B(E2)_{\rm in}$ in Table II, which are a factor of 10 smaller than the calculated ones. These ratios suggest that the $M1$ strength obtained with QTR is too large for ^{135}Pr as well.

The reproduction of the very small $B(M1)$ values is a problem for the QTR description of transverse wobbling. The mechanism for generating the $M1$ radiation is simple in the HFA. The magnetic moment $\vec{\mu} = g_j \vec{j}$ of the high-j particle is aligned with the s-axis. It wobbles together with the rotor generating the $M1$ radiation. The transition rate is given by the squared amplitude of this oscillation, which is determined by the wobbling amplitude of the rotor and the length of $\vec{\mu}$. As seen in Fig. 19, the HFA gives somewhat larger $B(M1)$ than QTR, which can be attributed to the HFA assumption of rigid alignment of the high-j particle with the s-axis. In the case of QTR, the coupling of the high-j particle is not rigid. Its $\vec{\mu}$ does not completely follow the motion of the rotor, which reduces the amplitude of its own wobbling motion and, as a consequence, the intensity of the $M1$ radiation. Hence, the $B(M1)$ values of QTR reflect the degree of alignment of the high-j particle with the short axis, i.e., the transverse character of the wobbling motion. We assume that the experimental $B(M1)$ values are substantially smaller than the calculated ones, because there are additional couplings between the rotor core and the quasiparticle that the QTR does not take into account (The CQP model considers only the coupling to the deformed quadrupole field.) This conjecture is supported by our study of transverse wobbling in the framework of QRPA in a forthcoming paper [27].

V. SUMMARY

Studying the classical orbits of the angular momentum vector of a triaxial rotor we have demonstrated that the presence of a high-j quasiparticle, which rigidly aligns its angular momentum $\vec{j}$ with one of the principal axes, drastically changes the motion of the coupled system. Two types of wobbling motion appear: the longitudinal and the transverse, depending, respectively, on whether the quasiparticle $\vec{j}$ is *aligned with* the axis of the largest MoI (*longitudinal wobbler*) or is oriented *perpendicular* to this axis (*transverse wobbler*). The assumption that the quasiparticle $\vec{j}$ is rigidly aligned with one of the principal axes (frozen alignment—FA) allowed us to derive simple analytical expressions for the wobbling frequency and $E2$ and $M1$ transition rates in analogy to the well-known formulas obtained by applying the harmonic approximation to the motion of the triaxial rotor [21] (harmonic

FA—HFA). Our simple HFA expressions help to understand why for the longitudinal alignment the wobbling frequency monotonically increases with the total angular momentum whereas it decreases for transverse alignment. There is a critical angular momentum where the transverse wobbling regime ends and the one- and zero-phonon bands merge into one $\Delta I = 1$ sequence. The simple HFA expressions provide a classification scheme for the wobbling motion and a qualitative understanding of the results obtained in the framework of the more realistic quasiparticle+triaxial rotor (QTR) model. All strongly deformed wobbling bands observed at high spin in the Lu and Tm isotopes carry the signature of transverse wobbling.

We studied the excitation energies and the electromagnetic $E2$ and $M1$ transition rates of transverse wobbling states in ^{163}Lu and ^{135}Pr in the framework of the QTR. The deformation parameters of the rotor were calculated by means of the micro-macro method. The three moments of inertia of the rotor were considered as free parameters, which were adjusted to fit the experimental energies of the zero- and one-phonon wobbling bands. Good agreement with the measured energies and $E2$ strengths was found for the high spin wobbling bands in ^{163}Lu, which has a strongly deformed triaxial shape. The signature of transverse wobbling, the decrease of the wobbling frequency with angular momentum, was reproduced. In accordance with experiment, the predicted critical spin of $I \approx 50$ of the transverse wobbling band is higher than the observed spins. The ratios between the three moments of inertia determined by the fit turned out to be close the ones calculated by means the cranking model. Assuming the ratios for irrational flow resulted in a much too low critical spin. Because the moments of inertia of the weakly deformed ^{135}Pr are smaller by a factor of about three, the wobbling bands appear lower spin. Fair agreement agreement of the QTR results with the measured energies and $E2$ strengths was found as well. At low spin the wobbling mode is transverse. At the critical spin of $I = 29/2$ the wobbling mode changes from transverse to longitudinal, which is caused by a realignment of the of the $h_{11/2}$ proton from the short to the medium axis. The ratios between the fitted moments of inertia did not agree with the ones obtained by assuming irrotational flow nor with the ones calculated by means the 3D-cranking model, both of which gave a too low critical spin. However for all three ways of determining the moments of inertia, the medium axis has the largest one, followed by the short axis, and the long axis.

In summary, the concept of transverse wobbling provides a natural explanation for the decrease of the wobbling frequency with increasing angular momentum and the enhanced $E2$ transitions between the wobbling bands. It is decisive that the ratios between the three moments of inertia of the triaxial rotor and the orientation of the odd quasiparticle are in qualitative agreement with microscopic calculations based on the cranking model.

ACKNOWLEDGMENTS

We thank J. Matta and U. Garg for providing us the tentative results of their measurements. The work was upported by U.S. DoE Grant No. DE-FG02-95ER4093.

APPENDIX

The relation between the QTR Hamiltonians in the laboratory and intrinsic frames of reference is established by transforming the coupling term $\sum_\mu q^*_\mu Q_\mu$ to the principal axis system of the core. Because this term is rotational invariant we obtain

$$\sum_\mu q^*_\mu Q_\mu = \bar{q}_0 \bar{Q}_0 + (\bar{q}_2 + \bar{q}_{-2})\bar{Q}_2. \tag{A1}$$

where $\bar{Q}_0$ and $\bar{Q}_2$ are the nonzero core quadrupole moments of the triaxial core. They can up to a scaling factor f be parametrized in terms of ε and γ as $\bar{Q}_0 = f\,\varepsilon\cos\gamma$ and $\bar{Q}_2 = f\,\varepsilon\cos\gamma/\sqrt{2}$. Defining the particle quadrupole moments as $q_\mu = r^2 Y^2_\mu$ the coupling term takes the familiar form of a triaxially deformed potential

$$\sum_\mu q^*_\mu Q_\mu = f\,r^2\big(\varepsilon\cos\gamma\,\bar{Y}^2_0 + \varepsilon\cos\gamma/\sqrt{2}\big(\bar{Y}^2_2 + \bar{Y}^2_{-2}\big)\big). \tag{A2}$$

The appropriate scaling factor f for obtaining the standard form of the deformed potential in the resulting Hamiltonian (9) is given by

$$\kappa\,f = \frac{2}{3}\sqrt{\frac{4\pi}{5}}\,\hbar\omega_\circ \approx 1.057\,\hbar\omega_\circ, \tag{A3}$$

where $\hbar\omega_\circ = 41A^{-1/3}$ MeV is the oscillator energy constant. Inserting the resulting coupling term in Eq. (25) we obtain the deformed quasiparticle term h_{dqp} of the QTR Hamiltonian (9). Expressing in the core part H_c the core angular momentum $\vec{R} = \vec{J} - \vec{j}$ in terms of the total a.m. and the particle a.m. gives the QTR Hamiltonian (9). The explicit transformation of the wave functions between the laboratory and intrinsic frames can be found in [21]. The coupling strength κ is related to the deformations ε and γ of the quasiparticle-core system by

$$\kappa\,\langle 0||Q||2\rangle = \hbar\omega_\circ\varepsilon\cos\gamma, \tag{A4}$$

where $\langle 0||Q||2\rangle$ means the reduced matrix element of the core quadrupole operator taken between the 0^+ ground state and the first 2^+ state of the core.

[1] L. D. Landau and E. M. Lifshits, *Mechanics* (Pergamon Press, New York, 1976).
[2] S. Golden and J. K. Bragg, J. Chem. Phys. **17**, 439 (1949).
[3] S. W. Ødegård *et al.*, Phys. Rev. Lett. **86**, 5866 (2001).
[4] D. R. Jensen *et al.*, Nucl. Phys. A **703**, 3 (2002).
[5] G. Schönwasser *et al.*, Phys. Lett. B **552**, 9 (2003).
[6] P. Bringel *et al.*, Eur. Phys. J. A **24**, 167 (2005).
[7] H. Amro *et al.*, Phys. Lett. B **553**, 197 (2003).
[8] G. Hagemann, Eur. Phys. J. A **20**, 183 (2004).
[9] D. J. Hartley *et al.*, Phys. Rev. C **80**, 041304(R) (2009).
[10] D. J. Hartley *et al.*, Phys. Rev. C **83**, 064307 (2011).
[11] Ikuko Hamamoto, Phys. Rev. C **65**, 044305 (2002).

[12] Ikuko Hamamoto and Gudrun B. Hagemann, Phys. Rev. C **67**, 014319 (2003).
[13] Kosai Tanabe and Kazuko Sugawara-Tanabe, Phys. Rev. C **73**, 034305 (2006).
[14] Kosai Tanabe and Kazuko Sugawara-Tanabe, Phys. Rev. C **77**, 064318 (2008).
[15] S. J. Zhu *et al*., Int. J. Mod. Phys. E **18**, 1717 (2009).
[16] M. Matsuzaki, Y. R. Shimizu, and K. Matsuyanagi, Phys. Rev. C **65**, 041303(R) (2002).
[17] M. Matsuzaki, Y. R. Shimizu, and K. Matsuyanagi, Phys. Rev. C **69**, 034325 (2004).
[18] M. Oi, Phys. At. Nucl. **70**, 1577 (2007).
[19] Y. R. Shimizu, T. Shoji, and M. Matsuzaki, Phys. Rev. C **77**, 024319 (2008).
[20] T. Shoji and Y. R. Shimizu, Progr. Theor. Phys. **121**, 319 (2009).
[21] A. Bohr and B. R. Mottelson, *Nuclear Structure*, Vol. II (Benjamin, New York, 1975), p. 190ff.
[22] S. Frauendorf, Nucl. Phys. A **677**, 115 (2000).
[23] F. Dönau and S. Frauendorf, Phys. Lett. B **71**, 263 (1977).
[24] A. Kerman and A. Klein, Phys. Lett. **1**, 185 (1962).
[25] H. J. Jensen *et al*., Nucl. Phys. A **695**, 3 (2001).
[26] J. Matta *et al*. (private communication, to be published in Phys. Rev. Lett.).
[27] F. Dönau and S. Frauendorf [Phys. Rev. C (to be published)].